## 3D GEOLOGICAL MODELLING

ERNST SCHETSELAAR[1]
[1] *Geological Survey of Canada, 615 Booth Street, Ottawa, Ontario, K1A 0E9*

Over 220 exploration and delineation boreholes totaling 195 linear km were used to build a detailed 3D geological model of the Lalor deposit that guided the interpretation of the 3D seismic data (Figure 9). Recent in-mine drill holes that focused on the ore zones were also used as 3D modeling constraints. The model covers an area of 2050 m by 1330 m around the drill-delineated ore lenses and extends down to a depth of 1500 m (see Figure 1 for outline of the 3D model). The various steps of the work flow for creating the 3D geological model are shown in Figure 7.

First, 3D geological surfaces, representing the contacts between the main lithostratigraphic units, were built (1 in Figure 7). These surfaces define the contacts between the hanging wall and footwall lithostratigraphic units of the Lalor deposit. Constraints used for modelling them included: (i) lithostratigraphic unit contacts extracted from the 1:20 000 scale geological map (Bailes and Galley, 2007) (ii) lithostratigraphic markers defined in a selected set of 17 reference drill holes (Bailes, unpublished report, 2013b) (iii) lithofacies intervals encoded from the detailed log descriptions of all the drill holes and (iv) bedding orientations restored from drill core angles between the drill core axis and intersected bedding (Figure 7). The sulphide ore lenses provided additional 'soft' constraints for validating and refining the footwall-hanging wall contact and the Chisel-Lalor structural break.

Second, a curvilinear grid model was built from the 3D geological surfaces using the structural knowledge-unified approach SKUA® (Mallet, 2004; 2 in Figure 7). This approach benefits from using a coordinate transformation (the UVT transform) that enables to condition stochastic grid modelling of categorical and continuous properties by the geometry of the host rock geological structure (Figure 8; Schetselaar, 2013). The 3D-modelled geological surfaces provided a complete partitioning of the volume of interest, yielding a total of 7 lithostratigraphic units (Figure 7).

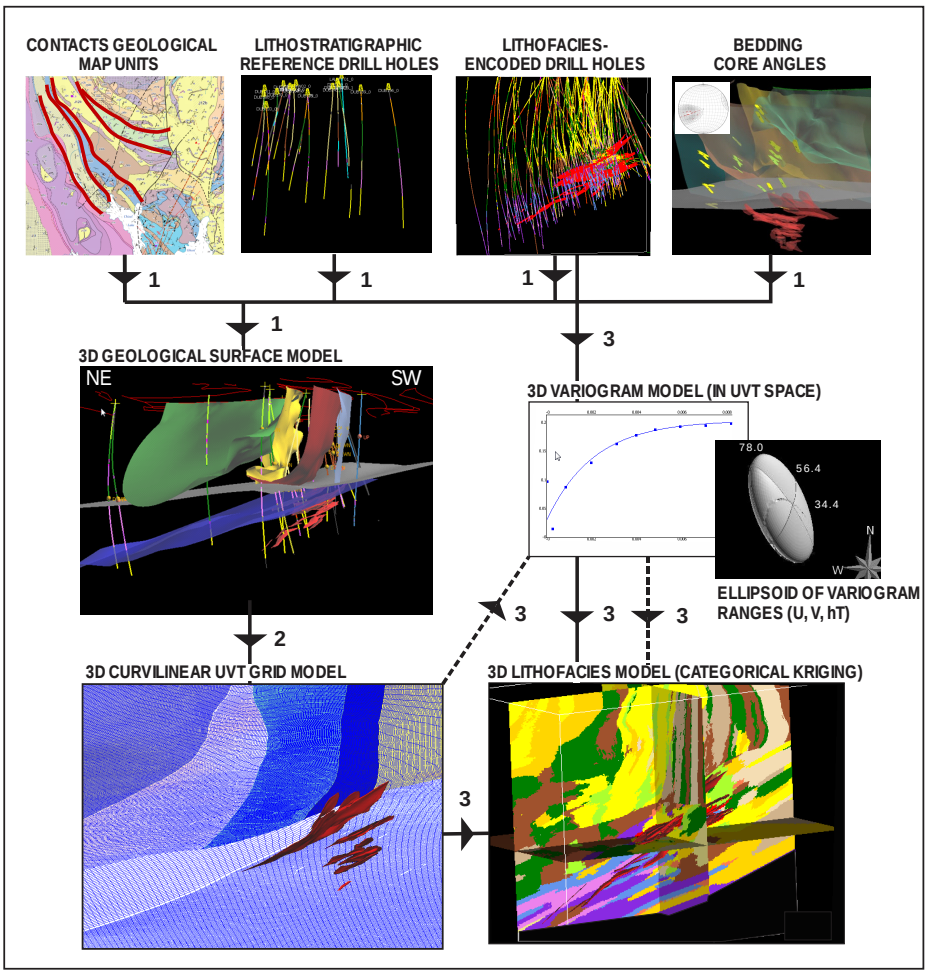


**Figure 7.** Work flow for building a 3D geologic surface and lithofacies grid model of the Lalor deposit. Numbers refer to the various processing steps discussed in the text.

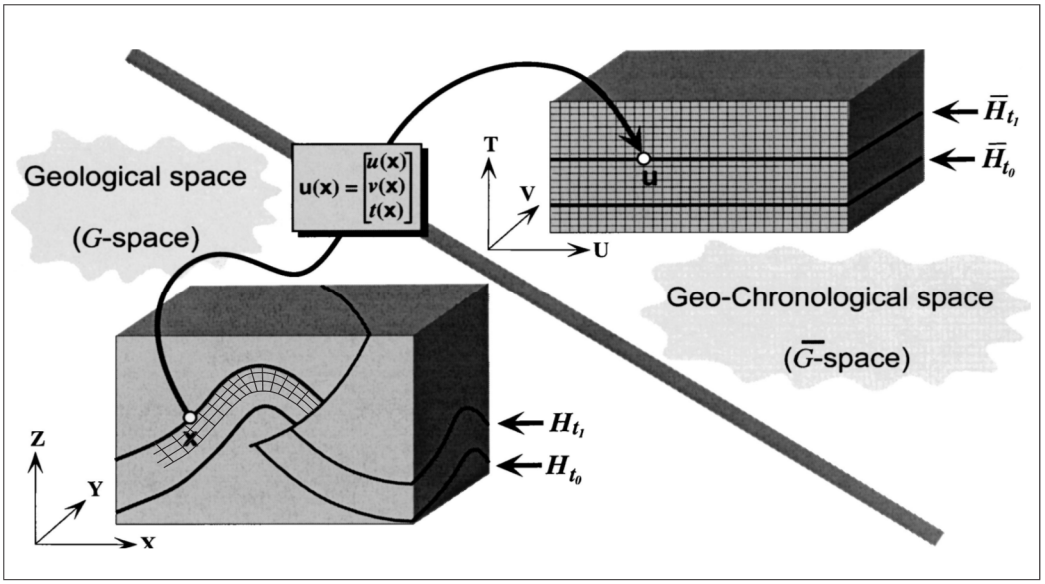


**Figure 8**. Transformation between Geological and Geochronological spaces to facilitate numerical grid modelling in complex geological settings (after Mallet, 2004). The faulted-curvilinear grid in Geological space becomes a Cartesian grid in geochronological space after applying the UVT transform, in which UV represent paleogeographic coordinates parallel to stratification and T represents geologic time normal to stratification. Since points of equal geologic time are by definition on a horizontal plane, the UVT transform 'flattens' out fold and fault structures, which facilitates stochastic modelling of continuous and categorical properties. The modelled-properties are mapped back on the curvilinear grid in geological space using the inverse UVT transform (Mallet, 2004).

Because the lithostratigraphic units could not be correlated across the Chisel-Lalor break, this contact was considered an angular unconformity in the topological encoding of the modelling work flow. This provided the best solution for honouring the distinct lithostratigraphic sequences in the footwall and hanging wall of the deposit, even though this contact is most likely of tectonic origin (Bailes *et al.*, 2013).

Third, class labels from a total of 15 lithofacies classes was mapped on the cells of the curvilinear grid by applying categorical kriging on a point set sampled at a spacing of 2 m along the lithofacies-encoded drill hole intervals (3 in Figure 7). This 15-fold lithofacies classification was based on the immobile $Zr/TiO_2$ immobile element ratio computed from drill hole lithogeochemistry, subdividing the samples into lithofacies of mafic, intermediate or felsic composition.

**Table 2.** Lithofacies classification for 3D modelling of the Lalor deposit based on $Zr/TiO_2$ immobile element ratio and textural and fabric observables in drill core.

| Main lithofacies group | $Zr/TiO_2$ | | Nr | CODE | Description |
|---|---|---|---|---|---|
| COHERENT VOLCANIC ROCKS | <=0.013 | | 1 | MAFVR | mafic volcanic rocks (basalt, andesite) |
| | > 0.013 & < 0.019 | | 2 | INTVR | intermediate volcanic rocks (dacite) |
| | >= 0.019 | | 3 | FELVR | felsic volcanic. rocks (rhyolite, rhyodacite) |
| COARSE-GRAINED VOLCANICLASTIC ROCKS (FRAGMENTALS) | <=0.013 | | 4 | VCLCM | mafic coarse-gr volcanicl. rocks (fragmentals) |
| | > 0.013 & < 0.019 | | 5 | VCLCI | interm. coarse-gr volcanicl. rocks (fragmentals) |
| | >= 0.019 | | 6 | VCLCF | felsic coarse-gr volcanicl. rocks (fragmentals) |
| FINE-GRAINED VOLCANICLASTIC ROCKS (LAPILLI TUFF / TUFF) | <=0.013 | | 7 | VCLFM | mafic fine-gr volcanicl. rocks (tuff/lapilli tuff) |
| | > 0.013 & < 0.019 | | 8 | VCLFI | interm. fine-gr volcanicl. rocks (tuff/lapilli tuff) |
| | >= 0.019 | | 9 | VCLFF | felsic. fine-gr volcanicl. rocks (tuff/lapilli tuff) |
| GNEISS /SCHIST (UNRECOGNIZABLE PROTOLITHS) | <= 0.013 | | 10 | GNSCHM | gneiss/schist mafic protolith |
| | > 0.013 & < 0.019 | | 11 | GNSCHI | gneiss/schist mafic protolith |
| | >= 0.019 | | 12 | GNSCHF | gneiss/schist mafic protolith |
| REMAINING LITHOFACIES CLASSES | | | 13 | ORE | sulphide ore |
| | | | 14 | ARG | Argillite |
| | | | 15 | DIO | feldspar-phyric diorite/gabbro |

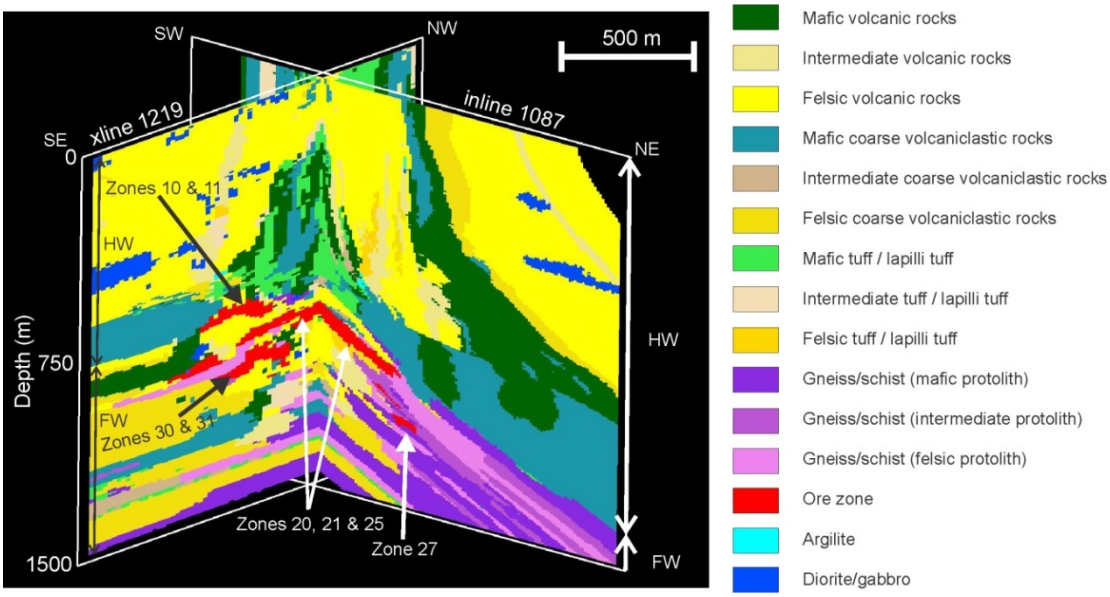


**Figure 9.** Perspective view to the west of the 3D litho-geological model used to constrain and support the interpretation of the 3D seismic data. The outline of the 3D model relative to the 3D seismic data is shown in Figure 1. Hanging wall units are steep especially above the ore zones. The least altered footwall rocks are shown in green and yellow whereas the most altered footwall rocks are in pink-to-purple tones. The two sections, which correspond to inline 1087 and crossline 1219 of the 3D seismic volume, provide a good overview of the main ore zones of the Lalor deposit. HW= hanging wall; FW=footwall.

Further subdivision of these three categories using fabric and textural descriptive attributes of drill core, resulted in the total of 15 lithofacies classes (Table 2). To support variable structural anisotropy in the distribution of each lithofacies unit, 3D variograms were estimated for each of the 15 lithofacies classes in the point set using an exponential variogram model.

Fourteen of the fifteen lithology classes were interpolated in UVT space using ordinary categorical kriging on grid cells of 20 m parallel to and 5 m normal to the stratigraphic layering to honour the geological structure of the footwall and hanging wall of the deposit. Only lithofacies class 15: mafic intrusive rocks (diorite and gabbro) which are often sub-horizontal and intrude the general structure, were kriged in a Cartesian coordinate system. Finally, all 15 interpolated lithofacies classes were resampled to a Cartesian voxet model with cubic grid cells to facilitate integration with the 3D seismic data (Figure 9). The lithofacies model is relatively accurate in the immediate vicinity of the boreholes but less reliable near the edges or at greater depth (i.e., near 1500 m) where the distribution of boreholes is sparse. An extensive overview on the 3D lithofacies grid modeling method can be found in Schetselaar (2013).

Figure 9 presents two cross-sections through the 3D lithofacies model which reveal the geological complexity of the area. Rocks forming the hanging wall are generally steeply-dipping near the surface but have shallower dips close to the contact with footwall rocks, particularly in the northeastern part of the model. Footwall rocks are everywhere moderately-dipping to the northeast. Footwall rocks with the most intense hydrothermal alteration (pink and purple units in Figure 9) were classified using the characteristics of the protolith rather than their actual metamorphic description (i.e., gneiss and schist). The protolith signatures were determined from the ratio of immobile elements ($Zr/TiO_2$) obtained from geochemical analysis available for cores from almost all boreholes (Floyd and Winchester, 1977; Caté *et al.*, 2013). This approach was used to help define the characteristics of the host rocks prior to metamorphism. This approach was not used for the footwall rocks towards the southwest which are also altered but not intensely enough to mask their volcanic origin (units in yellow and green in Figure 9). The model suggests an interfingered lateral transition between the most to least altered footwall rocks (Figure 9). Alternatively, a fold structure associated with a fault could explain the juxtaposition of moderately and highly altered footwall rocks (Caté *et al.*, 2014; Schetselaar and Shamsipour, 2015). Also note that many units in this model have a limited lateral extent and are discontinuous which complicates their imaging with seismic methods. Figure 9 also shows sulphide bodies (red) corresponding to five zinc zones (zones 10, 11, 20, 30, and 31), and three gold zones (zone 21, 25, and the gold-copper zone 27). In the 3D model, the ore zones are defined from the economical envelope used for the planning of the mine and therefore exclude non-economical mineralized intersections logged in several boreholes. Ore zones close to each other or overlapping are generally grouped as one zone in the model.